PHYSICAL REVIEW B **71**, 195308 (2005)

Heterointerface formation of aluminum selenide with silicon: Electronic and atomic structure of Si(111):AlSe

J. A. Adams,[1] A. Bostwick,[1] T. Ohta,[2] Fumio S. Ohuchi,[2] and Marjorie A. Olmstead[1,*]

[1]*Department of Physics, University of Washington, Box 351560, Seattle, Washington 98195, USA*

[2]*Department of Materials Science and Engineering, University of Washington, Box 352120, Seattle, Washington 98195, USA*

(Received 24 August 2004; published 9 May 2005)

In this paper we present a new, stable, unreconstructed surface termination of silicon, Si(111):AlSe. The structure forms the interface layer when aluminum sesquiselenide (Al_2Se_3) is deposited on Si(111) by molecular beam epitaxy. The atomic structure of the interface layer was investigated using angle-resolved valence and core-level photoelectron spectroscopy and diffraction. The Al_2Se_3/Si(111) interface forms an unreconstructed bilayer structure similar to GaSe-terminated Si, with Al directly above the top Si atom and Se over the hollow site, although the temperatures for bilayer formation and for Se re-evaporation from the film are higher for AlSe than for GaSe. In addition, the valence band structure shows that the AlSe bilayer electronically passivates the bulk Si, with all interface states lying within the bulk Si bands.

DOI: 10.1103/PhysRevB.71.195308 PACS number(s): 68.35.Bs, 73.20.At, 79.60.Jv

I. INTRODUCTION

Heteroepitaxy of dissimilar materials frequently leads to the formation of interface compounds with properties that are quite different from either the substrate or the overlayer. By forming the substrate for subsequent growth, these interface compounds strongly influence the structure and properties of the heteroepitaxial film. They also control electronic transport and atomic interdiffusion across the heterointerface. Of particular importance are the composition, thickness, structure, and stability of this interface layer.

A particularly important class of interface compounds are those that form a stable termination of the bulk substrate. Passivation of the Si(111) surface has been achieved through monolayer arsenic termination,[1,2] monolayer hydrogen termination,[3] and GaSe bilayer termination.[4–8] These passivation layers, by removing the adatoms and complex surface morphology of the Si(111) 7×7 reconstruction, provide ideal templates for heteroepitaxy. In addition to preventing interdiffusion and etching of the substrate by heteroepitaxial materials, they may also serve as an interface strain buffer or as a surfactant for further epitaxial growth. In this paper, we report on a new, stable, unreconstructed interface compound on silicon, Si(111):AlSe.

Heterostructures combining III-VI semiconductors with silicon have attracted attention[6–8] due to their close lattice matching and promising optoelectronic properties. For example, cubic Ga_2Se_3 has a band gap reported as 1.9 eV[9] or 2.6 eV[10] and a lattice constant only 0.3% smaller than silicon,[11] while layered GaSe has a 2.0 eV band gap and a hexagonal lattice parameter 2.4% smaller than Si(111).[12] Here we investigate Al_2Se_3 which has a 3.1 eV band gap[13] and a hexagonal lattice constant (3.89 Å) 1.3% larger than Si(111).[14] Aluminum sesquiselenide, Al_2Se_3, is of interest for heterostructures combining Al_2Se_3 and Ga_2Se_3, with the potential for a larger band gap analog to optoelectronic devices based on AlAs, GaAs, and the band gap engineering provided by Al_xGa_{1-x} alloys.[15] The selenides have the advantage of being latticed matched to silicon and, therefore, may be readily integrated with silicon-based technologies.

Al_2Se_3 is the least studied of the group III chalcogenides, with little published literature[13,14,16] and, to our knowledge, none on its compatibility with silicon or other members of the III-VI family of semiconductors. The stable bulk form of Al_2Se_3 is a defected wurtzite structure with 1/3 of the cation sites vacant. Ga_2Se_3 or In_2Se_3, on the other hand, form defected zincblende structures.[11,17] Both GaSe and InSe form a layered bulk structure whereas layered AlSe has not been reported in either bulk or thin film form.

In this paper, we investigate initial interface formation for Al_2Se_3 on Si(111), determining interface quality, stoichiometry, and structure. This information is essential to understand the growth process for further exploitation of Al_2Se_3, and for establishing the role of the interface layer as a buffer layer for heteroepitaxy.

Under a large range of growth conditions (500 °C $< T_{sub} <$ 750 °C and flux $<$4 Å/min), heteroepitaxial growth of Al_2Se_3 on Si(111) is inhibited after the formation of an initial bilayer. This AlSe bilayer forms an unreconstructed termination of the Si crystal and represents a new stoichiometry for aluminum selenide. At lower substrate temperatures and/or higher fluxes, thin film growth of wurtzite Al_2Se_3 is observed after completion of the first AlSe bilayer.[18] A similar self-terminating bilayer is observed for GaSe deposited on Si(111) at substrate temperatures between 500 °C and 550 °C.[4,5]

We have measured the atomic and electronic structure of the AlSe/Si(111) interface layer using energy and angle-resolved core and valence state photoemission. We find the Al and Se form an unreconstructed bilayer, with Al directly above the underlying Si, and Se over the hollow site, reflecting an extension of the cubic Si lattice rather than the wurtzite structure of bulk Al_2Se_3. Our measured Al-Se interface bond length is longer than that in bulk Al_2Se_3 or other tetrahedrally bonded Al-Se compounds. The bilayer has AlSe stoichiometry despite the Al_2Se_3 source material; thicker films[18] show stoichiometry closer to Al_2Se_3. The electronic structure of the passivated surface shows no states within the silicon

 ©2005 The American Physical Society

energy gap; the Se lone-pair state is located just below the Si valence band maximum.

The rest of this paper is organized as follows. First, we present a description of the experimental sample preparation and techniques (Sec. II). In Sec. III we describe the experimental results. We first present information on the symmetry and stoichiometry of the AlSe layer using core level photoemission spectroscopy and low energy electron diffraction (Sec. III A), followed by determination of the Al-Se bond length and direction using high kinetic energy photoelectron diffraction (Sec. III B). In Sec. III C we exploit the large backscattering amplitude of electrons at low kinetic energies to determine the Si-Al bond length and lateral registration between the bilayer and substrate using normal emission variable energy photoelectron diffraction. In Sec. III D we further probe the structure and symmetry of the interface layer with low kinetic energy angle dependent photoelectron diffraction. Finally, in Sec. III E we present the electronic structure of Si(111):AlSe obtained through angle-dependent valence band spectroscopy. The results are discussed in Sec. III and summarized in Sec. IV.

II. EXPERIMENTAL CONSIDERATIONS

We deposited thin films of aluminum selenide on Si(111) using molecular beam epitaxy (MBE). The substrates were cut from commercial *p*-type Si(111) wafers ($\rho \sim 1\ \Omega\,\mathrm{cm}$) and were prepared using the etching method of Shiraki.[19] Samples were outgassed in vacuum at 650 °C–750 °C for a minimum of 8 h. The Shiraki oxide was then removed by repeated annealing to $\sim 1000\ ^\circ\mathrm{C}$ for 5–10 s until a well-ordered 7×7 LEED pattern was observed. Samples were heated by direct current; the temperature was monitored using an optical pyrometer. The clean Si surface was free of carbon, oxygen and other residual elemental contaminants within an x-ray photoelectron spectroscopy detection limit of $\sim$0.05 ML.

Aluminum sesquiselenide was evaporated from Al_2Se_3 granules[20] heated in a pyrolytic boron nitride (PBN) crucible to temperatures between 900 °C and 940 °C, yielding a flux of $1-4$ Å/min, as measured by a quartz crystal monitor placed at the substrate position. The crucible temperature was measured using a thermocouple contacting the outside of the crucible. The silicon substrate temperature was held constant during deposition and was varied among the different samples between 500 °C and 750 °C. Deposition times ranged from 6 to 12 mins. After growth, the samples were transferred under ultrahigh vacuum from the MBE growth chamber to analysis chamber.

Al_2Se_3 readily reacts with water vapor through the reaction $Al_2Se_3 + 6H_2O \rightarrow Al(OH)_3 + 3H_2Se$. When source material has been exposed to air, such as when the Al_2Se_3 crucible has recently been filled, large bursts of pressure and flux are observed during initial degassing. Quadrupole mass spectrometry measurements indicate that the major constituent released is H_2Se. Some Se_2 is also detected. The chamber pressure and growth rate on the crystal monitor attenuate, and the flux settles to a repeatable value, once the cell has been heated to growth temperatures several times or for a long period of time (several hours). All growth experiments reported in this paper were performed after this initial outgassing to remove the reacted surface layer from the source material.

Photoemission experiments were performed both in Seattle, WA, using a Mg Kα x-ray source for x-ray photoelectron spectroscopy (XPS) and diffraction (XPD) measurements and a 21.2 eV He I discharge lamp for angle-resolved valence band photoemission, and in Berkeley, CA, using synchrotron radiation at beamline 7.0.1 of the Advanced Light Source (ALS). Base pressures of the experimental system in Seattle were 8×10^{-11} Torr in the deposition chamber and 3×10^{-10} Torr in the analysis chamber. At the Advanced Light Source (ALS), base pressures were 2×10^{-10} Torr in the deposition chamber and 1×10^{-10} Torr in the analysis chamber.

Core-level x-ray photoelectron spectroscopy (XPS), which is both element specific and sensitive to the local chemical environment, was utilized to determine the coverage and relative abundance of Al and Se and the number of local chemical environments for Al, Se and Si, and to monitor for possible interdiffusion or surface contamination. Low energy electron diffraction (LEED), with its sensitivity to long-range order and surface symmetry, was used to probe possible surface reconstruction, Al vacancy ordering or other regular surface features of the film.

We probed the local atomic structure to establish the orientation and arrangement of the bilayer using both high and low kinetic energy angle-resolved x-ray photoelectron diffraction. To discern the registry of the bilayer relative to the silicon substrate, as well as interatomic distances at the interface, we utilized multiple-scattering effects and backscattering, which are more apparent at low kinetic energies, measured by constant initial-state spectroscopy (CIS).

Additional information about interface quality was obtained by studying the valence electronic structure with angle-resolved photoelectron spectroscopy (ARPES). The valence band structure is sensitive to the long range atomic order of the film, contains information primarily from the top few layers of the sample, and reveals information about the chemical environment of atoms.

For experiments at the ALS, ARPES data were acquired using a Scienta-SES 100 display analyzer, which yields two-dimensional images of photoelectron intensity as a function of both energy and angle. Data were acquired as a series of intensity maps with angular width 10 deg, moving the sample 8 deg between images. Fifteen overlapping images were then stitched together to yield a single image map over the full angular range. This image $I(E,\theta)$ was then rescaled into $I(E,k_\parallel)$ for a subsequent analysis (and a presentation later in Fig. 6) via $k_\parallel = (1/\hbar)\sqrt{2mE_{\mathrm{kin}}}\sin\theta$, where the kinetic energy E_{kin} is related to the binding energy E as $E_{\mathrm{kin}} = h\nu - |E| - \phi$, and ϕ is the work function.

III. RESULTS AND ANALYSIS

A. Stoichiometry

Under a wide range of deposition conditions ($500\ ^\circ\mathrm{C} < T_{\mathrm{sub}} < 750\ ^\circ\mathrm{C}, 1$ Å/min $< R_{\mathrm{growth}} < 4$ Å/min), exposure of

Si(111) to Al_2Se_3 flux results in a single AlSe bilayer uniformly covering the surface, as described below. Additional exposure does not result in additional growth under these conditions. At higher flux and/or lower substrate temperature, growth does not self-terminate. However, under those growth conditions we find that the interface layer formed when growth is stopped at or below one bilayer has the same electronic and atomic structure as the self-terminated bilayer discussed here, showing the self-terminating bilayer to be the relevant surface for subsequent heteroepitaxy of Al_2Se_3.

Upon deposition of aluminum selenide, the low energy electron diffraction (LEED) pattern changes from the characteristic 7×7 pattern of clean Si(111) to a 1×1 pattern with sharp diffraction spots, low background intensity, and 3-fold symmetry. X-ray photoemission spectroscopy (XPS) measurements show the Se:Si ratio to be equal to that of the previously studied GaSe bilayer on Si(111),[4] indicating a full monolayer of Se. Adjusting for XPS cross sections,[21] the Al:Se ratio is between 1.0:1.0 and 1.0:1.2. This is significantly less Se than the 1:1.5 ratio of the source material (defected-wurtzite structure aluminum sesquiselenide).

High-resolution, surface sensitive ($h\nu=160$ eV) Al $2p$ and Se $3d$ core-level spectra show the presence of both elements in a single chemical environment (within an experimental resolution of 50 meV). Likewise, surface sensitive Si $2p$ core-level spectra show the silicon to be single component as well, within the experimental resolution.

The results strongly suggest that the interfacial bonding is between Si and Al, since selenium-silicon bonding would produce a Si $2p$ chemical shift to higher binding energy of at least 0.5 eV relative to the Si $2p$ bulk.[22] This is further supported by photoelectron diffraction measurements (see later). The single-component overlayer peaks indicate a sharp interface without interdiffusion. We can also conclude that if there are cation vacancies, either they are not ordered or the size of the ordered domains is less than about 20 nm, since ordering on a scale larger than this would produce a superstructure detectable by LEED. A $\sqrt{3}\times\sqrt{3}$ pattern attributed to Al vacancy ordering is observed on thicker Al_2Se_3 films.[18]

B. Bilayer structure

In this section we discuss the specific atomic structure of the Al and Se atoms in the uniform chemical environment established by the spectroscopy and LEED measurements. We utilize high kinetic energy, forward focusing, x-ray photoelectron diffraction (XPD) to determine the relative position of the Al and Se layers. In Sec. III C we utilize low kinetic energy, backscattering photoelectron diffraction to probe the Al-Si bonding.

The solid-line curves in Fig. 1 represent the integrated intensity of Mg Kα excited Se $3d$ (Fig. 1(a)) and Al $2p$ (Fig. 1(b)) as a function of the polar angle along $[11\bar{2}]$. At these high kinetic energies, forward focusing dominates most multiple scattering effects and highlights neighboring atoms along bond directions. Both Al and Se curves have been normalized to remove the angle-dependent transmission function of our experimental system.

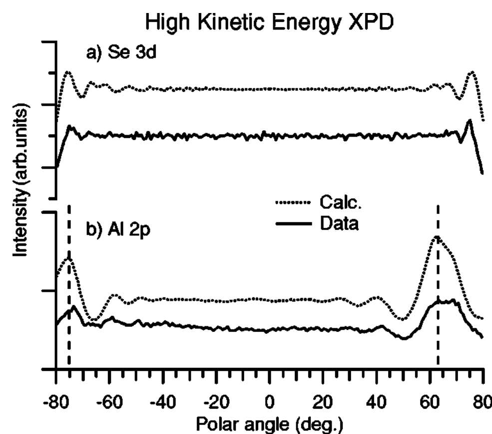

FIG. 1. Integrated photoemission intensity versus polar angle along the $[11\bar{2}]$ direction ($\theta>0$) and the $[\bar{1}\bar{1}2]$ direction ($\theta<0$) of the Si substrate for Mg Kα ($h\nu=1253.6$ eV) excited (a) Se $3d$, KE=1198 eV, and (b) Al $2p$, KE=1179 eV. Solid lines represent experimental data and dotted lines the calculated pattern using a selenium-on-aluminum bilayer model (see the text). Vertical dashed lines mark the Al-Se bond angle position along $11\bar{2}$ (+63.0 deg) and the Se along $\bar{1}\bar{1}2$ (−75 deg) determined from fitting the calculated pattern to the data.

The Se emission (the solid curve in Fig. 1(a)) shows no strong diffraction features except within about 15 deg of grazing emission. The weak features at high angles, ±75 deg, are first order diffraction peaks due to scattering from neighboring in-plane (90 deg) selenium atoms, with higher order scattering appearing at slightly lower angles.

The aluminum diffraction scan (the solid curve in Fig. 1(b)), is also flat and featureless at low angles. However, two strong peaks are present at high angles, the larger peak at about +63 deg and the smaller at about −76 deg. The size of the two peaks relative to other spectral features and the presence of the surrounding smaller peaks is strongly indicative of forward focusing. The smaller peaks at a slightly lower angle are the higher order diffraction rings of the main forward scattering peaks.

The presence of higher order diffraction peaks in the selenium curve suggests that the selenium layer is well ordered; however, the lack of any pronounced features indicates that the selenium layer has no ordered structure above it. The peaks in the aluminum diffraction scan, on the other hand, indicate forward focusing by Se atoms. Combining the Al and Se results, we deduce that the deposited film consists of a uniform Al layer beneath an ordered Se layer. Additionally, the asymmetry of the Al diffraction curve about normal emission implies that the film is a predominantly single orientation. The large peak located 63 deg toward $[11\bar{2}]$ from normal indicates the Al-Se bond is roughly parallel to a Si-Si bond in the diamond-structure substrate ("type A" orientation), a zincblende extension of the silicon bulk rather than the wurtzite orientation of bulk Al_2Se_3.

The bond angle, and hence the Al-Se bond length, may be determined by comparing the experimental data with simulated diffraction patterns. We have employed the multiple scattering calculation program MSCD (Ref. 23) to model the

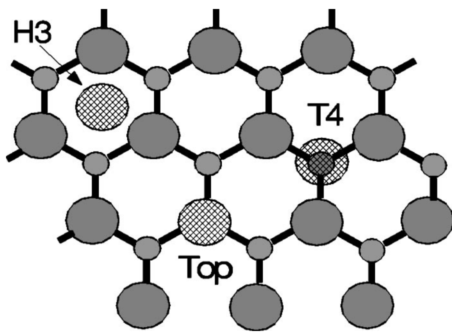

FIG. 2. Possible high-symmetry sites for Al on the Si(111) surface: Top, directly above a top layer Si atom; T_4, above a second-layer Si atom; and H_3, above a fourth-layer Si atom.

diffraction. Using the inferred selenium-on-aluminum bilayer structure and an in-plane spacing commensurate with the silicon substrate (required by the 1×1 LEED pattern), the Se-Al layer spacing was varied and the calculated curves for Al compared to the experimental data to obtain a quantitative best-fit value. The reliability factor, R, was minimized, where R is given by

$$R=\frac{\sum_i (\chi_{ci}-\chi_{ei})^2}{\sum_i (\chi_{ci}^2+\chi_{ei}^2)},$$

where χ_c and χ_e are the normalized intensities for the calculation and experiment, respectively, and are summed over each data point of the curve, i. χ is obtained following the method employed by the MSCD code: $\chi=(I-I_0)/I_0$ where I is the absolute intensity and I_0 is a background function derived from a smoothing of the absolute intensity.

The dotted-line curves in Fig. 1 are best fit ($R=0.035$ for Al) curves produced from a comparison of the calculated diffraction curves to the data. The Se-Al layer spacing is 1.13 ± 0.02 Å, corresponding to an Al-Se bond angle of 63.0 deg±0.4 deg from sample normal (highlighted with a dashed line in Fig. 1) and an Al-Se bond length of 2.49 Å.

This layer spacing is significantly larger than the average 0.78 Å spacing in bulk wurtzite Al_2Se_3, in which the Al-Se bond direction is 71 deg from (111). The smaller bond angle in the bilayer film can only partially be attributed to lateral compression that would cause the selenium layer to expand vertically, as that would typically conserve the bond length. The 2.49 Å measured Al-Se bond length is 0.15 Å longer than the average Al-Se bond length[24] in either Al_2Se_3 or Al_2ZnSe_4, indicating a change in the local bonding. One possible origin of this difference is the full aluminum layer, as opposed to the vacancy structure of the bulk crystals, preventing Se relaxation in the presence of vacancies. Another contributing factor may be a reduction in the ionicity of the Al-Si bond relative to the Al-Se bond in bulk Al_2Se_3.

C. Bilayer-substrate alignment

In this section we address bonding of the AlSe layer to the Si substrate. The absence of a measurable chemical shift of the interface Si $2p$ component precludes use of Si photoelectron diffraction to obtain information on Si-Al bonding. However, by taking advantage of multiple scattering effects at lower kinetic energies due to interference between the direct and scattered wave, we are able to utilize constant initial-state Al $2p$ photoemission to infer the local arrangement of neighboring atoms. In particular, a comparison of experimental and simulated normal emission Al $2p$ intensity as a function of photon energy (and hence electron wave vector) yields the lateral alignment of the Al with the Si substrate as well as the Al-Si spacing.

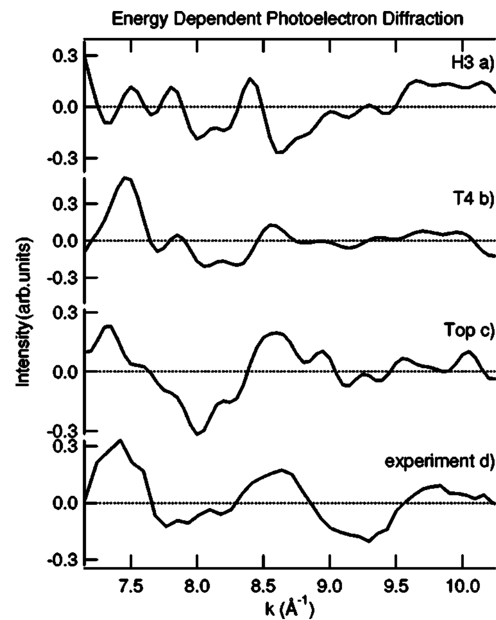

FIG. 3. Al $2p$ χ functions versus electron wave vector, k, taken normal to the sample surface. Calculated diffraction scans for aluminum occupying (a) an H_3 site, (b) a T_4 site, and (c) a Top site relative to the silicon surface. (d) Experimental energy-dependent photoelectron diffraction. The photon energy range for this data is 250 eV to 500 eV with 5 eV steps.

The three-fold symmetry observed in LEED, as well as in the stereographic XPD projections discussed in Sec. III D, requires that the Al atoms occupy one of three possible high-symmetry sites on the Si(111) surface shown in Fig. 2: H_3 (above a fourth layer silicon), T_4 (above a second layer Si), or top (above a top layer silicon). The XPD results of the previous section would then place the Se above the T_4, top, or H_3 sites, respectively. Intensity variations of normal-emission, Al $2p$ photoelectrons with respect to electron wave vector were calculated using MSCD for these three possible sites. For each symmetry site, the Al-Si layer spacing was varied. Then, a quantitative, best-fit R factor between the experiment and simulation was obtained using the same method as for the XPD curves in Fig. 1. Figures 3(a)–3(c) show the best-fit χ functions determined for each site. Figure 3(d) shows the normalized experimentally measured Al $2p$ variation χ_e. For both the experimental and calculated curve the normalized intensity, χ, was obtained following the method described in Sec. III B.

A quick glance at the calculated curves shows the best qualitative agreement for the top site; R-factor analysis finds

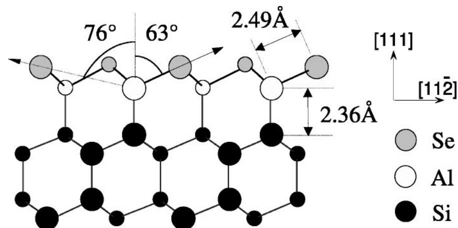

FIG. 4. Experimentally determined structural parameters for the AlSe bilayer on the Si(111) surface.

the data and calculation also have the best quantitative agreement for the Al in the top site. A summary of the determined structural parameters is shown in Fig. 4. The determined Si-Al bond length of 2.36 ± 0.02 Å is much smaller than the Al-Si bond length in Si(111):Al($\sqrt{3}\times\sqrt{3}$), 2.49 Å,[25] but the relationship is similar to that between the Ga-Si bond length in Si(111):GaSe, 2.35 Å,[5] and Si(111):Ga($\sqrt{3}\times\sqrt{3}$), 2.50 Å.[26]

D. Surface structure symmetry

Additional information about the element-specific structure and symmetry of the surface may be obtained through the full angular dependence of the photoemission intensity. Figure 5 shows the measured (left) and calculated (right) stereographic projection of the Se 3d (top) and Al 2p (bottom) photoemission intensity at photon energy $h\nu=320$ eV (KE=245 eV for Al; KE=265 eV for Se).

The pattern depicts the integrated intensity of the respective core-level emission at each angle; the sampled points were evenly distributed in solid angle. In the Al patterns (Fig. 5(c) and Fig. 5(d)) the strongest features arise from forward scattering by the overlying Se, centered at the same angles as the peaks seen above in the high-energy polar angle scan (line scan in Fig. 1 is equivalent to a vertical line through the origin in Fig. 5). Secondary diffraction rings are also visible. At these lower kinetic energies (relative to Fig. 1), multiple-scattering and backscattering are more apparent.

The Se diffraction pattern shows a mottled pattern attributed primarily to the scattering from in-plane Se atoms. The Se stereographic projection, like the high kinetic energy angle scan in Fig. 1(a), contains no prominent features indicative of forward focusing. The pattern is similar to that for Se in Si(111):GaSe, with a full multiple scattering calculation required to reproduce all the experimental features.[5]

Simulated diffraction patterns for the same atomic positions deduced from Figs. 1 and 3 (and shown in Fig. 4) are shown on the right hand side of Fig. 5. A comparison of the data and calculations indicates that the input parameters determined above through XPD and CIS are consistent with the data here. Additionally, the three-fold symmetry observed in the hologram agrees with that seen in the LEED pattern. The presence of subtle diffraction features at similar angles in both experiment and calculation indicate that the surface is well ordered and that the bilayer is primarily of a single orientation.

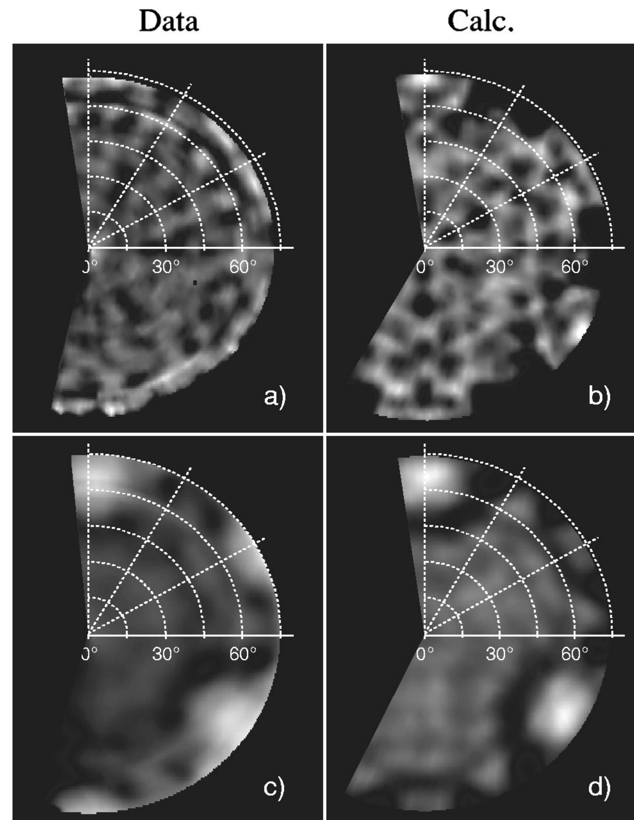

FIG. 5. Low kinetic energy holograms for Se 3d (a) experiment and (b) theory, and Al 2p (c) experiment and (d) theory. White indicates the greatest intensity and black the lowest intensity.

E. Valence band structure

The valence band for bilayer AlSe on Si(111) along $\bar{\Gamma}-\bar{K}-\bar{M}$ was measured with angle-resolved photoemission spectroscopy (ARPES), using both synchrotron radiation ($h\nu=130$ eV, Figs. 6 and 7) and a He I source $h\nu=21.2$ eV, Fig. 7(b). As described in Sec. II, several overlapping $I(E,\theta)$ images have been merged in angle, and then rescaled from angle to parallel momentum ($k_{\|}$), to produce the composite intensity distribution as a function of binding energy and parallel momentum along $[1\bar{1}0]$ shown in Fig. 6. The $\bar{\Gamma},\bar{K}$ and $\bar{M}$ points of the surface Brillouin zone are denoted by the solid black vertical lines. At this photon energy, 130 eV, $k_{\|}=0$ corresponds to the bulk Γ point in the fourth Brillouin zone (the bulk valence band maximum). The escape depth at this energy is $\sim$3–4 Å, maximizing the surface sensitivity.

The solid white lines overlaid on the image depict the boundary of the calculated bulk Si projected bands (integrated over $k_{\perp}$ for a particular $k_{\|}$). The areas shaded with vertical bars are forbidden regions of the bulk Si bands. The dots are the calculated emission for bulk Si. The full Si band structure was produced from a simple pseudopotential calculation utilizing the three, nonvanishing pseudopotential form factors for a diamond structure,[27] and the bands along the scan direction were derived from the calculated full band structure assuming a free electron final state and an inner potential of 11 eV.

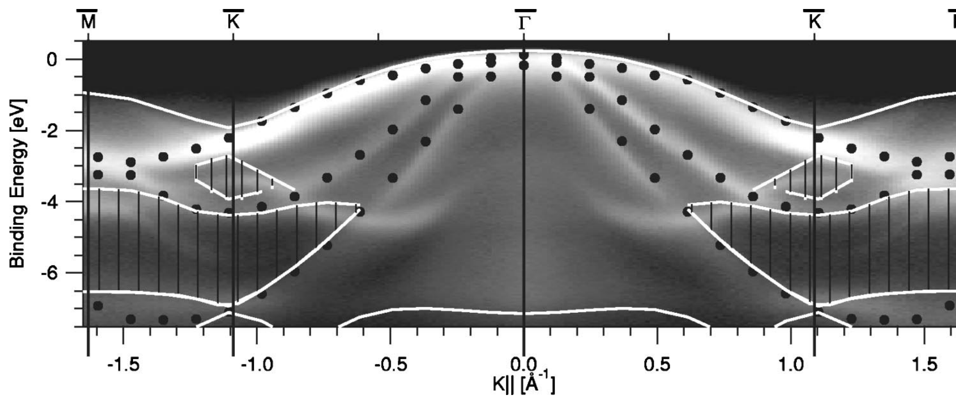

FIG. 6. Valence band of an AlSe bilayer on Si(111) in the $[1\bar{1}0]$ and $[\bar{1}10]$ directions, $\bar{\Gamma}-\bar{K}-\bar{M}$. Solid white lines represent the boundaries of the calculated Si projected bulk bands, with vertical black stripes marking forbidden regions below the valence band maximum. Dots represent the calculated bulk Si valence band emission along the scan direction. Photon energy $h\nu = 130$ eV.

In addition to bulk Si states, we expect additional bands from the surface termination. Electron counting arguments based on the Si(111):AlSe atomic structure predict a doubly occupied lone pair orbital on the Se similar to that for As on the Si(111):As surface.[2] In addition to the lone pair state, we expect states from within the terminating layer, the Se-Al bonds, and from the interaction of the bilayer with the substrate, the Al-Si bond.

In Fig. 6, the positions of the calculated Si bands all coincide with states in the measured band structure, indicating the near-surface silicon is in a very bulklike environment. The sharp, well-defined states show that there is very little scattering at the surface, indicating a well-ordered surface.

The local intensity maxima (spectral peaks) in Fig. 6 are plotted as open circles in Fig. 7. The solid lines on the left side of Fig. 7 are the calculated bulk Si valence emission (shown as dots in Fig. 6). We see excellent agreement for these states, plus additional bands not associated with bulk Si, highlighted as bold open circles. The assignment of these features as surface states and resonances is confirmed by comparison with data taken with the same parallel momentum and different perpendicular momentum (i.e., different photon energy), shown in Fig. 7(b).

The states represented by solid lines in Fig. 7(b) are the measured band structure (bulk and surface contributions) of Si(111):AlSe taken at $h\nu = 21.2$ eV using a He I source. The two different photon energies, 130 eV and 21.2 eV, correspond to different positions within the bulk Brillouin zone. Therefore, features which appear as overlapping open circles and solid lines in Fig. 7(b) highlight states that do not disperse with changing $k_\perp$; they therefore are associated with the bilayer termination, i.e., surface states and resonances. Note that all the bold data points (taken at $h\nu = 130$ eV) fit this description, as does the topmost band in region A. The true surface states fall within the forbidden regions of the bulk Si projected bands, the B region of Fig. 7.

The uppermost surface state (bold circles in region A of Fig. 7) is associated with the Se lone pair, as it has similar dispersion and location to the As and Se lone pair states for Si(111):As and Si(111):GaSe, respectively.[2,28–30] As mentioned above, electrons emitted at $k_\parallel = 0$ with $h\nu = 130$ eV are at Γ in the Si bulk Brillouin zone, which is the Si valence band maximum. Here the Si band-edge overlaps the Se lone pair state. At this energy, the lone pair state is only visible as a separate resonance in the second surface zone (bold circles in Fig. 7), and is, therefore, difficult to resolve. With 21.2 eV excitation, however, the highest bulk state at $k_\parallel = 0$ is about an eV lower, and the topmost state (solid line) is the lone pair emission. A comparison of the bulk calculation (lines in Fig. 7(a)) and the 21.2 eV data (lines in Fig. 7(b)) with the 130 eV data (topmost open circles dispersing downward from the

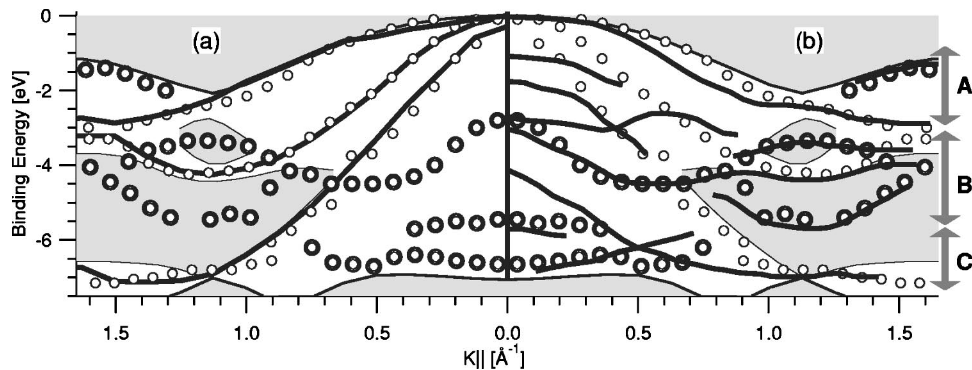

FIG. 7. Valence band of an AlSe bilayer on Si(111) in the $[1\bar{1}0]$ and $[\bar{1}10]$ directions, $\bar{\Gamma}-\bar{K}-\bar{M}$. Open circles are the plotted peak positions from the image in Fig. 6. Shaded regions are forbidden regions in the calculated Si projected bulk bands. Solid lines on the left half of the graph are the calculated Si bulk emission along the scan direction at $h\nu = 130$ eV (shown as dots in Fig. 6). Solid lines on the right half of the graph are the measured band structure of the bilayer on the silicon taken with He I, $h\nu = 21.2$ eV. Bold open circles are those that do not overlap a silicon bulk state on the left, but note that they do correspond with a state observed at the same $k_\parallel$ and different $k_\perp$ on the right—indicative of their two-dimensional nature.

valence band maximum (VBM)) shows the single observed peak to lie between the (calculated) bulk and (21.2 eV data) surface states. We thus assign it to the overlap of the Se lone pair with the Si band edge. We observe no occupied states in the bulk Si band gap for this passivated surface. Since Al_2Se_3 has such a large band gap (3.1 eV), it is expected that the AlSe/Si termination has no states within the Si band gap.

The surface-associated states in Region B (bold circles, 3–5 eV below the VBM) pass through or near forbidden regions in the bulk Si bands. Calculations of similar states for Si(111):As attribute these states to Si-As backbonds[2] and in Si(111):GaSe to Ga-Se p_x-p_y orbitals;[28] the equivalent states for this system are Al-Se bonds. One of these three bonds lies in the plane of measurement, leading to two separate states away from the zone center (~3 eV binding energy at $\bar{\Gamma}$). Region C, consisting of deep states 6-8 eV below the VBM are most likely Si-Al bonds, as they have similar energy and dispersion to Ga-Ga bonds in layered GaSe[31,32] and similar states were attributed to Si-Ga bonds in Si(111):GaSe.[28]

IV. SUMMARY

AlSe bilayer terminated Si(111) represents a new stoichiometry for aluminum selenide compounds and a new means to remove dangling bonds and surface reconstruction from Si(111). We have used high-resolution photoemission and photoelectron diffraction to investigate the composition, structural, and electronic properties of this system.

The local chemical environment closely resembles that of the GaSe bilayer on silicon despite differences in the bulk crystal structure of Al and Ga selenides. The Al sits directly above the top layer silicon with the Al-Se bond 63° toward $[11\bar{2}]$, so that the single-orientation interface bilayer follows the zincblende form, contrary to the stable wurtzite form of the bulk. The interface silicon is in a bulklike environment, similar to the isoelectronic structures Si(111):As, Si(111):H and Si(111):GaSe. The electronic structure shows extremely sharp states, indicating a well-ordered surface with no occupied states in the silicon band gap.

The high-temperature stability, high degree of order and absence of dangling bonds makes Si(111):AlSe a good candidate as a low surface energy growth platform for heteroepitaxy of next-generation silicon-based self-assembled nanostructures.

ACKNOWLEDGMENTS

The authors thank Dr. Eli Rotenberg and the ALS Beamline 7 staff for their expert input and assistance. This work was supported by NSF Grant No. DMR-0102427. Some of the research was conducted at the Advanced Light Source, which is supported by the U.S. Department of Energy under Contract No. DE-AC03-76SF00098 at Lawrence Berkeley National Laboratory.

*Electronic address: olmstd@u.washington.edu

[1] M. A. Olmstead, R. D. Bringans, R. I. G. Uhrberg, and R. Z. Bachrach, Phys. Rev. B **34**, 6041 (1986).
[2] R. I. G. Uhrberg, R. D. Bringans, M. A. Olmstead, R. Z. Bachrach, and J. E. Northrup, Phys. Rev. B **35**, 3945 (1987).
[3] G. S. Higashi, Y. J. Chabal, G. W. Trucks, and K. Raghavachari, Appl. Phys. Lett. **56**, 656 (1990).
[4] S. Meng, B. R. Schroeder, and M. A. Olmstead, Phys. Rev. B **61**, 7215 (2000).
[5] S. Meng, B. R. Schroeder, A. Bostwick, M. A. Olmstead, E. Rotenberg, and F. S. Ohuchi, Phys. Rev. B **64**, 235314 (2001).
[6] R. Fritsche, E. Wisotzki, A. Thissen, A. Islam, A. Klein, W. Jaegermann, R. Rudolph, D. Tonti, and C. Pettenkofer, Surf. Sci. **515**, 296 (2002).
[7] K. Ueno, H. Shirota, T. Kawamura, T. Shimada, K. Saiki, and A. Koma, Appl. Surf. Sci. **190**, 485 (2002).
[8] Y. Zheng, A. Koebel, J. Petroff, J. Boulliard, B. Capelle, and M. Eddrief, J. Cryst. Growth **162**, 135 (1996).
[9] K.-H. Park, H.-G. Kim, W.-T. Kim, C.-D. Kim, H.-M. Jeong, K.-J. Lee, and B.-H. Lee, Solid State Commun. **70**, 971 (1989).
[10] S. Morley, M. von der Emde, D. R. T. Zahn, V. Offermann, T. L. Ng, N. Maung, A. C. Wright, I. B. Fan, G. H. Poole, and J. O. Williams, J. Appl. Phys. **79**, 3196 (1996).
[11] D. Lübbers and V. Leute, J. Solid State Chem. **43**, 339 (1982).
[12] N. C. Fernelius, Prog. Cryst. Growth Charact. Mater. **28**, 275 (1994).
[13] E. Kauer and A. Rabenau, Z. Naturforsch. A **13**, 531 (1958).
[14] A. Schneider and G. Gattow, Z. Anorg. Allg. Chem. **277**, 49 (1954).
[15] A. Franciosi and C. G. Van de Walle, Surf. Sci. Rep. **25**, 1 (1996).
[16] K.-J. Range and H.-J. Hübner, Z. Naturforsch. B **28**, 353 (1973).
[17] J. Ye, S. Soeda, Y. Nakamura, and O. Nittono, Jpn. J. Appl. Phys., Part 1 **37**, 4264 (1998).
[18] J. A. Adams, Ph.D. thesis, University of Washington, 2004.
[19] A. Ishizaka and Y. Shiraki, J. Electrochem. Soc. **133**, 667 (1986).
[20] Obtained from ESPICorp Inc., Ashland, OR.
[21] J. J. Yeh and I. Lindau, At. Data Nucl. Data Tables **32**, 1 (1985).
[22] R. D. Bringans and M. A. Olmstead, Phys. Rev. B **39**, 12 985 (1989).
[23] Y. Chen, F. J. Garcia de Abajo, A. Chasse, R. X. Ynzunza, A. P. Kaduwela, M. A. Van Hove, and C. S. Fadley, Phys. Rev. B **58**, 13 121 (1998).
[24] *Crystal Data; Determinative Tables*, edited by J. D. H. Donnay and H. M. Ondik (United States National Bureau of Standards, Washington, 1973), 3rd ed.
[25] P. S. Mangat, K. M. Choudhary, D. Kilday, and G. Margaritondo, Phys. Rev. B **44**, 6284 (1991).
[26] A. Kawazu and H. Sakama, Phys. Rev. B **37**, 2704 (1988).
[27] P. Y. Yu and M. Cardona, *Fundamentals of Semiconductors: Physics and Materials Properties* (Springer-Verlag, Berlin, 1995).
[28] R. Rudolph, C. Pettenkofer, A. A. Bostwick, J. A. Adams, F. S.

Ohuchi, M. A. Olmstead, B. Jaeckel, A. Klein, and W. Jaegermann, New J. Phys. (to be published.)

[29] M. O. D. Camara, A. Mauger, and I. Devos, Phys. Rev. B **65**, 125206 (2002).

[30] M. O. D. Camara, A. Mauger, and I. Devos, Phys. Rev. B **65**, 205308 (2002).

[31] G. Margaritondo, J. E. Rowe, and S. B. Christman, Phys. Rev. B **15**, 3844 (1977).

[32] L. Plucinski, R. L. Johnson, B. J. Kowalski, K. Kopalko, B. A. Orlowski, Z. D. Kovalyuk, and G. V. Lashkarev, Phys. Rev. B **68**, 125304 (2003).